

Article

# Novel Cu and Pd-Cu Catalysts Supported on Multi-Walled Carbon Nanotubes for Steam Reforming and Decomposition of Methanol

Paweł Mierczyński <sup>1,\*</sup>, Agnieszka Mierczyńska-Vasilev <sup>2</sup>, Waldemar Maniukiewicz <sup>1</sup>, Krasimir Vasilev <sup>3</sup>  
and Małgorzata Szykowska-Józwiak <sup>1</sup>

<sup>1</sup> Institute of General and Ecological Chemistry, Lodz University of Technology, Zeromskiego 116, 90-924 Lodz, Poland

<sup>2</sup> The Australian Wine Research Institute, Waite Precinct, Hartley Grove cnr Paratoo Road, Urrbrae, Adelaide, SA 5064, Australia

<sup>3</sup> College of Medicine and Public Health, Flinders University, Bedford Park, SA 5042, Australia

\* Correspondence: pawel.mierczynski@p.lodz.pl; Tel.: +48-42-631-31-25

**Abstract:** In this study, multi-walled carbon nanotubes (MWCNTs) were prepared by chemical vapour deposition (CVD) using acetylene as a carbon source over an iron catalyst. As-prepared MWCNTs were used to support modern mono-copper, palladium, and bimetallic palladium-copper catalysts, and their feasibility for hydrogen production was tested during steam reforming of methanol (SRM) and methanol decomposition (DM). The structural characteristics of the MWCNTs were evaluated using the SEM and XRD methods. The physicochemical properties of the monometallic and bimetallic catalysts were analysed using the TPR and XRD methods. The promotion effect of palladium on methanol conversion rate and H<sub>2</sub> productivity in the case of the copper catalysts was demonstrated. The enhanced activity of the Cu/MWCNTs after palladium promotion was due to the formation of Pd-Cu alloy compound.

**Keywords:** bimetallic catalysts; hydrogen production; MWCNTs; decomposition of methanol; steam reforming of methanol



**Citation:** Mierczyński, P.; Mierczyńska-Vasilev, A.; Maniukiewicz, W.; Vasilev, K.; Szykowska-Józwiak, M. Novel Cu and Pd-Cu Catalysts Supported on Multi-Walled Carbon Nanotubes for Steam Reforming and Decomposition of Methanol. *Catalysts* **2023**, *13*, 533. <https://doi.org/10.3390/catal13030533>

Academic Editor: Leonarda Liotta

Received: 3 January 2023

Revised: 28 February 2023

Accepted: 1 March 2023

Published: 6 March 2023



**Copyright:** © 2023 by the authors. Licensee MDPI, Basel, Switzerland. This article is an open access article distributed under the terms and conditions of the Creative Commons Attribution (CC BY) license (<https://creativecommons.org/licenses/by/4.0/>).

## 1. Introduction

The intense increase in fuel prices and the dwindling of oil and coal stocks have increased interest in a new energy source [1,2]. One of the most promising alternative fuels is hydrogen. It can be easily produced at low temperature and under atmospheric pressure [3–5]. The current state of knowledge indicates that the synthesis of hydrogen during the steam-oxygen reforming reaction of methanol needs to be explored. In particular, the direct use of hydrogen in a direct methanol fuel cell (DMFC) is at issue [6]. The high energy density of methanol and the fact that the methanol oxidation process can be carried out relatively easily at low temperatures lead to the generation of low power off the grid. The electricity generated can be used for, e.g., battery chargers, digital cameras, mobile phones, and laptop repairs. Great hopes rest on the development of a fuel cell technology with hydrogen as an energy carrier [7]. The use of hydrogen in transport and stationary applications is receiving a great deal of technical and political attention [8]. Hydrogen is being explored for use in IC engines and fuel cell electric vehicles [9]. Fuel cell technology is in the initial stages of commercialisation and offers more efficient hydrogen use [10]. A hydrogen fuel cell vehicle offers advantages over hydrogen-fuelled IC engines [2,11]. Hydrogen and fuel cells are often considered as key technologies for future sustainable energy supply. Compared to traditional methods for electricity generation from coal, a fuel cell has lower carbon dioxide emissions (40–60%) and lower nitrogen oxide emissions (50–90%). The most used catalysts for the methanol-reforming reaction are

copper-based catalysts. High copper dispersion, high metal surface area values, and small particle size are the targets for achieving highly active catalysts. In the literature, many works have studied the addition of promoters [12–16] and the influence of preparation methods [17–20] on the catalytic properties of copper-supported catalysts. Despite the high activity and selectivity of copper catalysts (CuO/ZnO and CuO/ZnO/Al<sub>2</sub>O<sub>3</sub>) in methanol-oxidizing reactions, there are still ongoing studies concerned with their yield, selectivity, and enhancement of their stability [21]. Additionally, an exchange system that is active in the reforming of methanol is palladium catalyst. It is an effective decomposition catalyst that selectively forms H<sub>2</sub> and CO when supported on metal oxide [22–26]. However, when palladium is supported on ZnO, a high selectivity for CO<sub>2</sub> in the SRM reaction has been reported [27]. The formation of Pd-Zn alloys may explain this change in selectivity [28]. These palladium alloys are formed at moderate temperatures under reducing conditions [29,30]. An important key role in any process is the choice of support for catalytic systems. Typical support materials for methanol-reforming catalysts are SiO<sub>2</sub>, Al<sub>2</sub>O<sub>3</sub>, MCM-41, carbon black, ceramic slices, etc. There is little information in the literature dealing with the use of carbon nanotubes as supports for preparing catalytic systems for the reforming of methanol. The attractive properties of this material dictate the use of CNT as a carrier for methanol-reforming catalysts [31,32]. Furthermore, catalysts on CNT supports can be produced by various processes: impregnation, precipitation, colloidal reaction, electroless plating, and hydrothermal processes [32]. The main advantages of using CNTs as a catalyst support are their high specific surface area, high thermal and mechanical stability, specific interaction at the support–metal interface, adsorption of active catalytic nanoparticles in immersion and on the outer wall of the CNT, and ability to be chemically modified. The good conductivity of carbon nanotubes promotes the ‘spillover effect’ at the interface created by the active site [33]. Nanoparticles of the active phase that are distributed on the functional surface of the support (CNT) ensure that the created active sites are easily accessible to the reactants. The abovementioned properties of CNTs can directly influence catalytic activity and selectivity [34–39]. In this study, we investigated the promoting effects of palladium on copper catalysts supported on multi-walled carbon nanotubes (MWCNTs). In addition, this work also investigated the possibility of using MWCNTs prepared by the CVD method. The influence of adding palladium to copper catalysts on their reactivity and physicochemical properties in methanol reforming (SRM) and methanol decomposition was also studied in this work.

## 2. Results and Discussion

### 2.1. Characterization of the MWCNTs

Multi-walled carbon nanotubes were synthesised by chemical vapour deposition (CVD) at 850 °C using ferrocene as a source of iron catalyst. The obtained material was then characterized using a scanning electron microscopy (SEM) with energy-dispersive X-ray analysis (see Figure 1 and Table 1). The obtained SEM images recorded at different magnifications clearly confirm the formation of carbon nanotubes. In addition, it should be emphasised that inside of the MWCNT structure, iron species (Fe<sub>3</sub>C and α-Fe<sub>2</sub>O<sub>3</sub>) particles are present. The presence of these iron species on the surface and in the structure of the multi-walled carbon nanotubes is confirmed by TPR and XRD experiments [40]. The surface composition of the synthesised MWCNTs collected from the reactor was also evaluated using the SEM-EDX technique, and the results are presented in Table 1. The results confirm the existence of iron species on the MWCNTs’ surface.

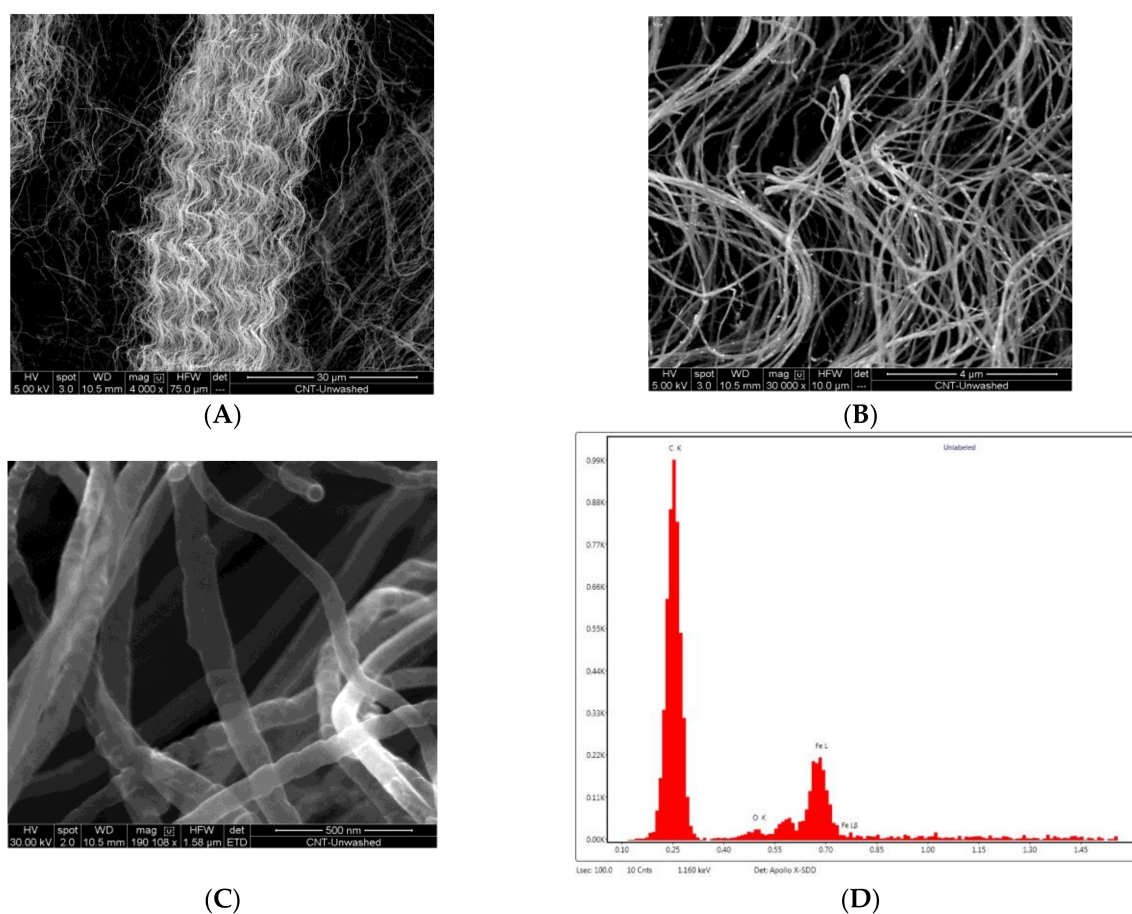


**Figure 1.** SEM (A–C) images and EDX (D) spectrum of multi-walled carbon nanotubes collected from the reactor.

**Table 1.** Element composition of the pristine MWCNTs from the EDX analysis.

No.	Element	(Atomic %)
1	C	90.67
2	O	1.92
3	Fe	7.41

## 2.2. Phase Composition Studies

The XRD diffraction spectra of the monometallic palladium, copper, and bimetallic Pd-Cu supported catalysts after their calcination in static air at 350 °C for four hours and after the SRM reaction are shown in Figure 2. For the copper- and copper-doped palladium catalysts, only after calcination at 350 °C, the XRD patterns (see Figure 2) show diffraction peaks at 31.5°, 37.0°, 44.9°, 59.6°, and 65.5°, corresponding to the crystal phase of CuO, and a relatively sharp peak between 20° and 30° due to the graphite-like phase. Moreover, the formation of the Fe<sub>3</sub>C (2θ = 37.7°, 37.8°, 42.9°, 43.8°, 44.6°, 45.0°, 45.9°, and 49.1°) and α-Fe<sub>2</sub>O<sub>3</sub> (2θ = 24.2°, 33.2°, 35.7°, 40.9°, 49.5°, 54.1°, 62.5°, and 64.0°) phases are seen in all catalysts supported on the MWCNTs prepared during the CVD synthesis. This is consistent with the results presented in a previous paper [40]. The diffraction peaks originating from the PdO crystalline phase are observed in the diffraction curve for the calcined monometallic palladium catalyst. In contrast, the diffraction curve recorded for the bimetallic Pd-Cu catalyst calcined under static air does not show any diffraction peaks that can be assigned to the PdO phase. These results indicate that the palladium oxide particles in the case of

the bimetallic system are too small to be detected by the XRD technique [41,42]. In the case of the 1%Pd/MWCNT catalyst after steam reforming of methanol, the diffraction peaks assigned to the graphite-like phase and the  $\text{Fe}_3\text{C}$ , Pd, and magnetite phases are detected. The XRD curves of the mono-Cu and bimetallic Pd-Cu catalysts tested in SRM process show the presence of diffraction peaks originating from the graphite-like phase, and the  $\text{Fe}_3\text{C}$ ,  $\text{Fe}_3\text{O}_4$ , metallic copper, CuO, and  $\text{Cu}_2\text{O}$  phases, respectively. In our previous work [43], we also investigated the phase composition of a mono-Cu and a bimetallic Pd-Cu catalyst on binary oxide support after calcination and reduction processes. The results showed a metallic copper phase and an alloy phase (Pd-Cu) formed after reduction. The alloy phase formed was responsible for the high selectivity during the steam reforming of methanol process [43]. In this work, the diffraction curves of the catalysts after the activation process and reaction show the presence of the following phases: graphite-like phase,  $\text{Fe}_3\text{C}$ ,  $\text{Fe}_3\text{O}_4$ , CuO,  $\text{Cu}_2\text{O}$ , and Cu. The lack of the metallic palladium phase in the case of the tested bimetallic catalysts could be because an alloy phase between the two elements Pd and Cu is also formed, which plays a crucial role in the SRM process.

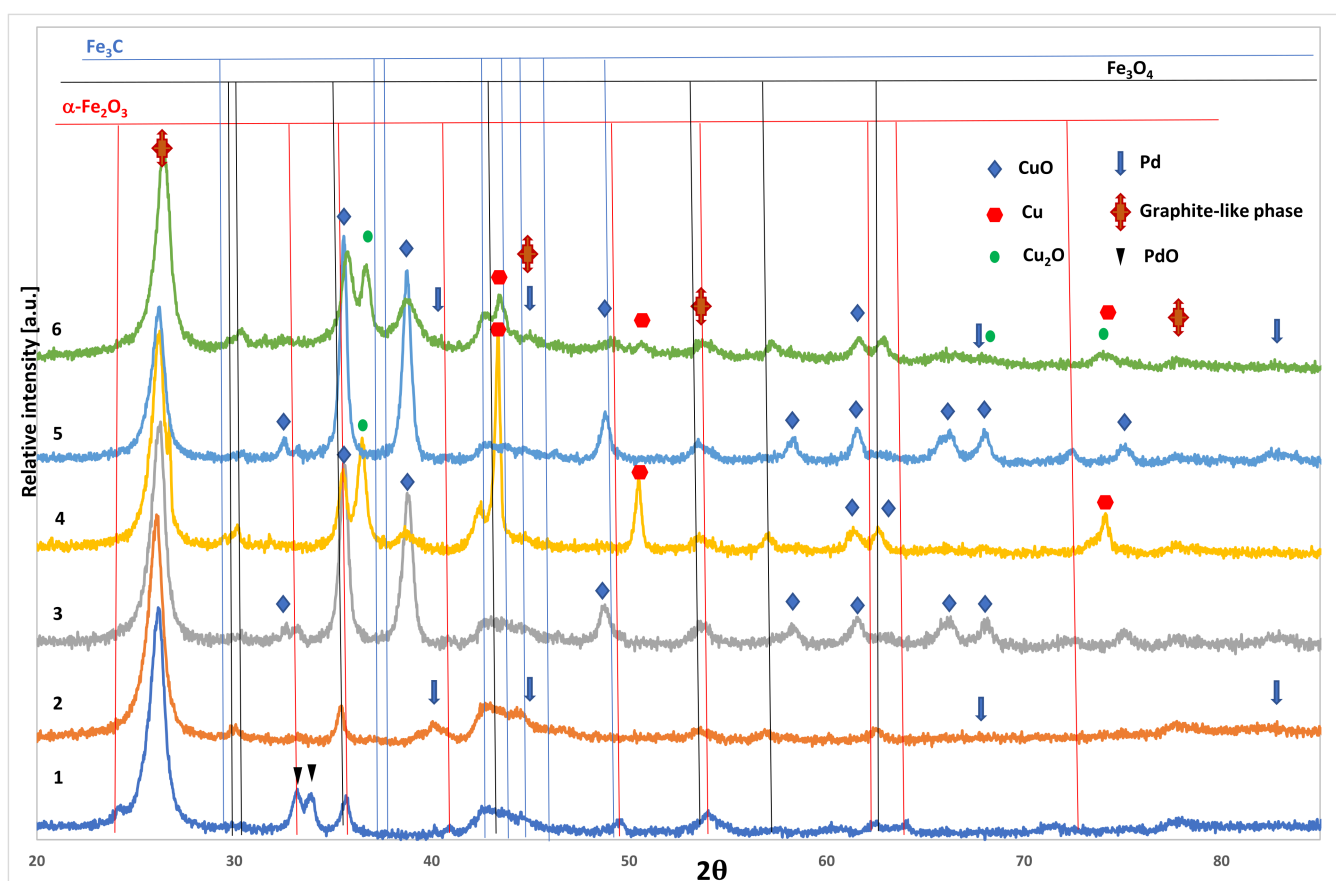


**Figure 2.** The XRD diffractograms for the monometallic Pd and Cu and the bimetallic Pd-Cu supported catalysts calcined under static air for 4 h at 350 °C and after steam reforming of methanol reaction: (1) 1%Pd/MWCNTs calcined under static air at 350 °C for 4 h, (2) 1%Pd/MWCNTs after SRM process, (3) 20%Cu/MWCNTs calcined under static air at 350 °C for 4 h, (4) 20%Cu/MWCNTs after SRM process, (5) 1%Pd-20%Cu/MWCNTs calcined under static air at 350 °C for 4 h, and (6) 1%Pd-20%Cu/MWCNTs after SRM process.

In our previous work, the same results were reported [43]. Moreover, in this work, we saw the formation of the  $\text{Cu}_2\text{O}$  phase for the catalysts only after steam reforming of methanol. Xiong et al. [44] investigated cobalt catalysts supported on CNTs and carbon spheres during Fisher–Tropsch synthesis. They also did not see any diffraction peaks

on the XRD curves attributed to the cobalt particles due to their small size. The XRD measurements also show a broad diffraction peak between the Bragg lines of Pd (1 1 1) and Cu (1 1 1) after the reduction and SRM reactions in the case of the bimetallic catalysts. This result further confirms that the formation of a Pd-Cu alloy phase in the case of a bimetallic catalyst is the presence of broad diffraction peaks at  $2\theta$  in the range of  $35\text{--}39^\circ$ . Lambert et al. [45] studied the phase composition of Pd-Cu/SiO<sub>2</sub> co-gelled xerogel catalysts. They also detected the alloy formation between Pd and Cu. The authors confirmed the alloy formation from the appearance of a broad peak between the (1 1 1) Bragg lines of Pd and Cu. The authors attributed the appearance of this diffraction peak to the formation of the alloy phase. Neyertz et al. [42] reported copper incorporation into the palladium particle or alloy formation, which was confirmed by the shift of the diffraction peak to values of  $2\theta$  higher. The formation of Pd-Cu alloy was also seen in the case of carbon-supported Pd-Cu catalysts for the system reduced under a hydrogen atmosphere at elevated temperatures ( $>773\text{ K}$ ). The authors claimed that the presence of the broad characteristic diffraction peaks assigned to Cu and C (support) phases, located at  $2\theta = 43.3$  and  $43.7$  [46], confirms the formation of an alloy phase between Pd and Cu. In this work, we also observed a broad diffraction peak between  $2\theta$  angle of  $43.3^\circ$  and  $43.7^\circ$  in the case of the bimetallic catalyst tested in SRM process, what further confirms the alloy formation.

### 2.3. Reduction Studies

The reducibility of mono- and bimetallic catalysts was examined using temperature-programmed reduction (TPR-H<sub>2</sub>). The TPR profiles of the monometallic and bimetallic supported catalysts are shown in Figure 3. The TPR profiles of the monometallic copper and palladium catalysts show three or four hydrogen consumption peaks depending on the catalysts. The TPR profile of the palladium catalysts shows four hydrogen reduction peaks. The first effect is related to the reduction in the PdO phase. The second reduction peak situated in the temperature range of  $220\text{--}300^\circ\text{C}$  is attributed to the reduction of hematite formed in the structure of the MWCNTs during the preparation of the support material. The third reduction peak with the maximum hydrogen consumption rate situated at  $500^\circ\text{C}$  is assigned to the methanation of the MWCNTs, together with the reduction of magnetite to metallic iron. The last hydrogen consumption peak that is hardly visible on the TPR profile above  $550^\circ\text{C}$  is associated with further methanation of the carbon nanotubes. Xiong et al. [44] investigated the reduction behaviour of cobalt catalysts supported on carbon nanotubes. They also saw a high-temperature reduction peak at about  $500^\circ\text{C}$ , which was attributed to the catalytic decomposition of the support. The reduction studies for monometallic copper catalysts showed three hydrogen consumption peaks in the temperature range of  $180\text{--}560^\circ\text{C}$ . The effect in the temperature range of  $180\text{--}380^\circ\text{C}$  is attributed to the reduction of copper (II) oxide and hematite that are incorporated into the structure of the carbon material. The second peak with the maximum hydrogen consumption rate at about  $500^\circ\text{C}$  is attributed to the methanation of the MWCNTs and the magnetite reduction process. The last hydrogen consumption peak that is visible on the TPR-H<sub>2</sub> profile is attributed to the methanation of the carbon nanotubes. The TPR profile recorded for the copper catalyst promoted by palladium also shows three resolved reduction effects. The first two reduction effects are connected to the same copper and iron oxide species reduction observed for the copper supported catalysts, while the last hydrogen consumption peak that is hardly visible on the TPR-H<sub>2</sub> profile above  $550^\circ\text{C}$  is assigned to the methanation of the carbon nanotubes. It is worth noting that the addition of palladium to the copper catalyst generates a ‘spillover effect’ that explains the shift of the first reduction peak into the lower temperature range [47,48]. During the reduction process, the adsorbed hydrogen dissociates from the hydrogen atoms on the palladium surface. It passes from palladium to copper oxide, which facilitates the reduction of copper (II) oxide species (see Figure 3).

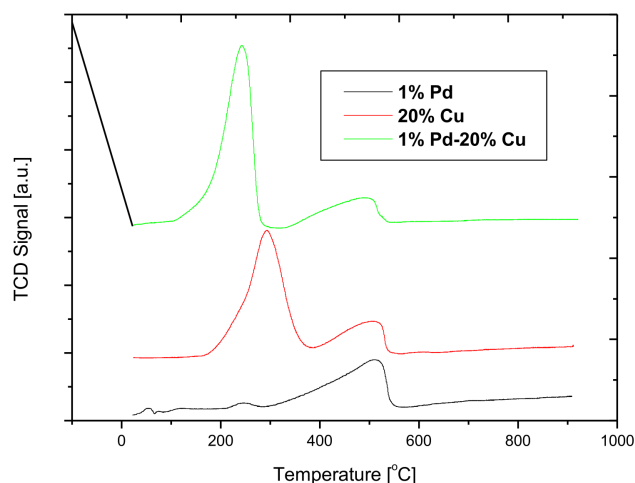


**Figure 3.** The TPR-H<sub>2</sub> of the monometallic (Cu, Pd) and bimetallic Pd-Cu catalysts supported on MWCNTs.

#### 2.4. Catalytic Activity

The effects of the addition of palladium to the copper catalyst and the activation procedure (reduction in a mixture of 5% H<sub>2</sub>-95% Ar) on the reactivity of the investigated catalytic material during steam reforming of methanol and decomposition of methanol were studied in detail. The temperature characteristics of the catalytic activity of the mono-Pd and Cu and bimetallic Pd-Cu supported catalysts during the steam reforming of methanol are shown in Figure 4 and Table 2.

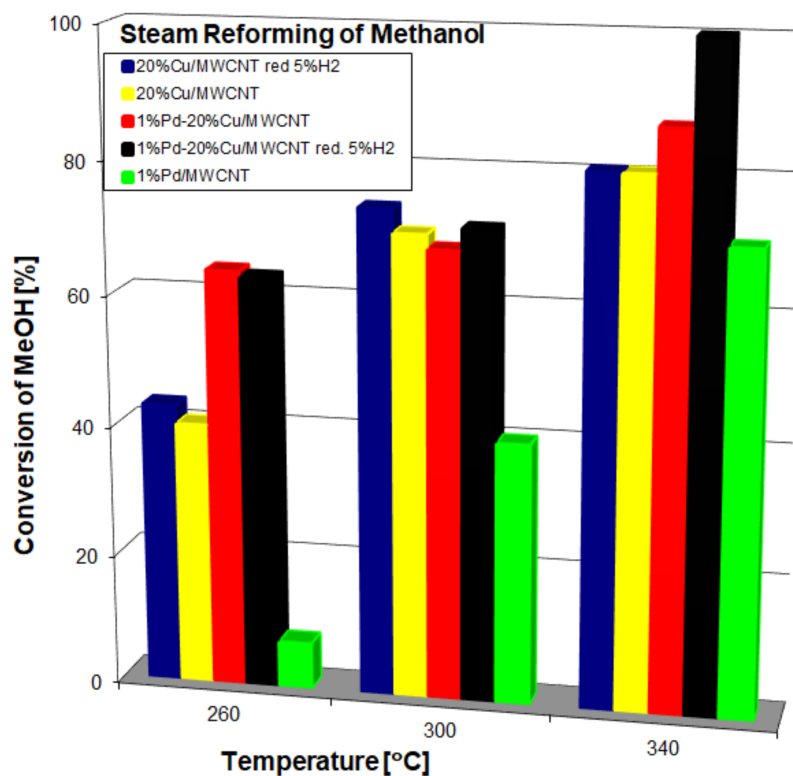


**Figure 4.** The methanol conversion results obtained for the monometallic and bimetallic catalysts during the steam reforming of methanol reaction.

**Table 2.** The catalytic activity results obtained for the monometallic copper and the bimetallic Pd-Cu/MWCNTs catalysts evaluated during the steam reforming of methanol.

Catalysts <sup>a</sup>	Temp. (°C)	Conv. of CH <sub>3</sub> OH(%)	Y <sub>H<sub>2</sub></sub> (%)	S <sub>CO</sub> (%)	S <sub>CO<sub>2</sub></sub> (%)
1%Pd/MWCNT <sup>b</sup>	260	7	71	76	-
	300	40	75	53	35
	340	70	70	60	30
20%Cu/MWCNT <sup>b</sup>	260	40	76	12	82
	300	70	78	12	87
	340	80	83	17	83
20%Cu/MWCNT <sup>c</sup>	260	43	92	28	69
	300	74	87	45	51
	340	80	97	40	58
1%Pd-20%Cu/MWCNT <sup>b</sup>	260	63	67	31	23
	300	68	73	33	37
	340	87	75	12	76
1%Pd-20%Cu/MWCNT <sup>c</sup>	260	63	75	45	51
	300	72	100	49	51
	340	100	90	28	70

<sup>a</sup> Reaction conditions: 0.1 g of catalyst, H<sub>2</sub>O:CH<sub>3</sub>OH = 1, temperature range 260–340 °C, and atmospheric pressure.

<sup>b</sup> Catalytic activity tests conducted over the calcined catalysts. <sup>c</sup> Catalytic tests performed over the catalysts after calcination and activation process in a mixture of 5%H<sub>2</sub>-95% Ar at 300 °C.

The activity result clearly shows that the methanol conversion value reaches 100% for the bimetallic 1%Pd-20%Cu/MWCNTs system activated at 300 °C for one hour in a reductive mixture (5%H<sub>2</sub>-95%Ar). It is worth noting that all catalysts activated in a mixture of 5%H<sub>2</sub>-95%Ar prior to the catalytic activity test exhibit higher methanol conversion compared to the non-activated catalysts. The lowest activity during the SRM process is shown by the monometallic palladium catalyst, which exhibits a methanol conversion of 7% at 260 °C and the lowest hydrogen yield at this temperature. It is worth noting that the palladium catalyst shows high selectivity for CO formation at this temperature. The other carbon-containing compounds formed at this temperature are methane, dimethyl ether, and methyl formate.

The activity measurements conducted for the monometallic catalysts show that the activation process improves the catalytic activity of the studied material. The monometallic catalysts activated in a reductive mixture showed higher methanol conversion values and higher hydrogen yield in the studied temperature range. In contrast, lower selectivity for CO<sub>2</sub> formation was observed for the activated copper catalyst. In addition, methane, methyl formate, and dimethyl ether were formed as by-products during the process for both activated and calcined samples. Furthermore, the measurements of the catalytic activity during the SRM process clearly showed that the promotion of copper catalysts by palladium positively influenced the catalytic activity of the investigated Cu/MWCNT system. Higher methanol conversion and hydrogen selectivity values were found for the calcined copper catalysts promoted by palladium. It is also worth noting that the activation process of the bimetallic catalyst further improves the catalytic activity and hydrogen selectivity. The only drawback of the results obtained for the calcined Pd-Cu catalyst is an improvement in the selectivity for CO and other products formed during the reaction carried out at 260 and 300 °C, respectively. In the case of the activated bimetallic catalyst on MWCNT supports, higher selectivity for the formation of hydrogen and CO<sub>2</sub> was detected at 260 and 300 °C, respectively.

The performance of the methanol decomposition reaction, which is expressed as methanol conversion, is shown in Table 3 and Figure 5. The activity tests performed for the calcined catalysts showed that the maximum methanol conversion was observed at 260 °C for all systems. The catalytic activity results showed that the less active catalyst

was the palladium system. The product distributions during the methanol decomposition reaction showed that carbon dioxide was not formed during the process realized on the calcined copper and copper-palladium catalysts and an activated copper catalyst at 200 °C. It was also confirmed that the activated mono- and bimetallic catalysts showed higher methanol conversion values compared to the non-activated systems at both temperatures. The calcined palladium and copper catalysts showed the highest hydrogen yield. The most active system was the bimetallic Pd-Cu/MWCNTs catalyst activated in a mixture of 5% $H_2$ -95%Ar, which showed a hydrogen yield equal to 90 and 89% at 200 and 260 °C, respectively. An alloy formation between Pd and Cu also explains the highest activity of this system in the decomposition of methanol. An alloy phase formation was confirmed by the XRD and TPR measurements. Furthermore, the reduction studies conducted for the bimetallic catalysts confirmed the 'spillover effect' between palladium and copper (II) oxide species. The confirmation of an alloy phase formation is the shift of the reduction effect assigned to the reduction of CuO towards a lower temperature range as a result of the dissociation of molecular hydrogen on the surface of the palladium particles to atomic hydrogen, which flows to the surface of copper (II) oxide and facilitates its reduction. Various variants of catalyst activation before activity tests can be found in the literature. Some authors reported that highly active systems with high dispersion and large specific surface area proceed to reduction at low temperatures [49]. There is no linear correlation between activity and reduction temperature, but more easily reducible systems have higher activity. However, other authors claim that catalysts that are more difficult to reduce are more active [17]. Jones et al. [50] reported that a catalyst with the highest reduction temperature has the best activity. In our case, the activity results clearly showed that the activation process, which was conducted before the activity tests, has an impact on the activity of the mono- and bimetallic systems tested in both reactions. The reduction process generates a 'spillover effect' between Pd and CuO, and in the final stage, an alloy formation. The resulting alloy changes the transfer of electrons between the components of the alloy. In addition, the presence of carbon nanotubes and the 'spillover effect' in the Pd-CuO/MWCNT systems can destabilise CuO bonds and facilitate the reduction process of CuO to Cu, which improves the activity [51,52]. Our activity studies confirmed that the reduction process leads to an improvement in the activity of the investigated catalysts in the studied processes. We previously tested MWCNTs [40] prepared via the CVD method in the oxy-steam reforming of methanol process. The activity results showed that the MWCNTs themselves are an active material of the investigated process. The results also showed that the activation process performed in a mixture of 5% $H_2$ -95%Ar has an important influence on the catalytic activity of the carbon nanotubes and their phase composition. In addition, it is also proven that the purification process of the MWCNTs has a huge influence on their reactivity properties in the studied reaction. In other works [53,54], we also studied the influence of noble metal addition on the catalytic activity of copper catalysts during oxy-steam reforming of methanol. The activity results showed that the addition of gold into the copper catalyst had an enormous effect on catalyst activity and selectivity in the studied reaction. The high activity and selectivity of the Au-Cu catalyst was explained by an alloy formation. In other work [55], the authors investigated copper catalysts promoted by Pd in the partial oxidation of methanol. The results showed that Pd-Cu alloy was formed during the reduction of the bimetallic catalysts at 300 °C or even below. In addition, the kinetic studies showed that the addition of palladium decreased the activation energy for steam reforming of methanol, which agrees well with our activity results. Nomoto et al. [56] studied Cu and Pd-Cu catalysts in the autothermal reforming of methanol process after calcination and after reduction. In the case of the autothermal reforming (ATR) of methanol process carried out on the copper catalysts, only trace amount of hydrogen production was detected. The XRD diffractograms recorded for this system do not show any diffraction peaks assigned to the metallic copper. This means that copper (II) oxide species are not reduced during the oxidative steam reforming of methanol process. In the case of the Pd-Cu catalysts, for both the calcined and reduced catalysts, the authors observed a higher

yield of hydrogen production rate in the studied process, and in the case of the bimetallic catalysts activated in a reducing mixture at 300 °C, the highest hydrogen production rate was observed. In addition, the XRD pattern recorded for the Pd-Cu catalyst after the ATR process shows the existence of diffraction peaks assigned to the metallic copper phase. It should also be noted that even if, during the ATR process, oxygen is consumed during the combustion and/or partial oxidation of methanol, a small amount of hydrogen is produced via the reforming and/or decomposition processes as a result of the effective use of exothermic heat. This result also confirms that palladium assists in the reduction process of copper (II) oxide species via the ‘spillover effect’ and explains the highest hydrogen yield observed in the case of the bimetallic catalysts. We obtained similar results, which confirm the ‘spillover effect’ between Pd and CuO species and the formation of an alloy between Pd and Cu.

**Table 3.** The catalytic activity results obtained for the monometallic copper and bimetallic Pd-Cu/MWCNTs catalysts during the decomposition of methanol reaction.

Catalysts <sup>a</sup>	Temp. (°C)	Conv. of CH <sub>3</sub> OH (%)	Y <sub>H<sub>2</sub></sub> (%)	S <sub>CO</sub> (%)	S <sub>CO<sub>2</sub></sub> (%)
1%Pd/MWCNT <sup>b</sup>	200	3	95	96	-
	260	86	96	88	11
20%Cu/MWCNT <sup>b</sup>	200	32	78	94	-
	260	90	93	81	12
20%Cu/MWCNT <sup>c</sup>	200	36	71	91	-
	260	100	72	84	16
1%Pd-20%Cu/MWCNT <sup>b</sup>	200	43	77	59	13
	260	100	87	75	17
1%Pd-20%Cu/MWCNT <sup>c</sup>	200	60	90	84	15
	260	100	89	84	15

<sup>a</sup> Reaction conditions: 0.1 g of catalyst, temperature range 200–260 °C, and atmospheric pressure. <sup>b</sup> Catalytic activity tests conducted over the calcined catalysts. <sup>c</sup> Catalytic tests carried out over the catalysts after calcination and activation process in a mixture of 5% H<sub>2</sub>-95% Ar at 300 °C.

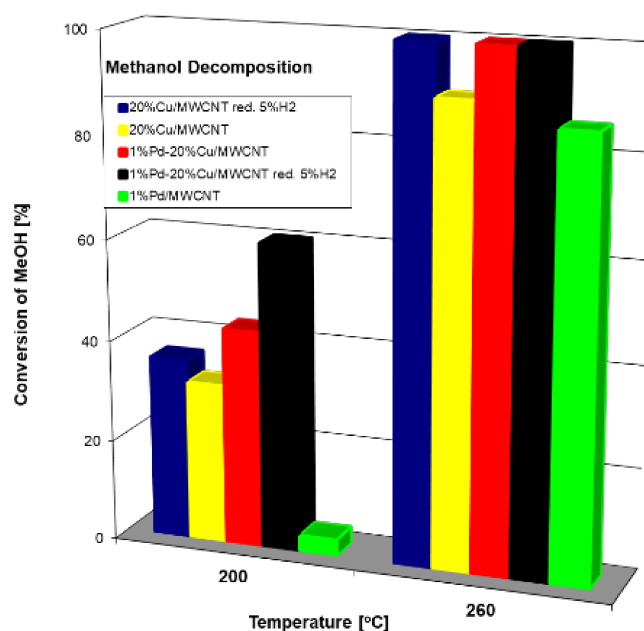


**Figure 5.** The methanol conversion results obtained for the monometallic and bimetallic catalysts during the methanol decomposition reaction.

### 3. Materials and Methods

#### 3.1. Catalytic Material Preparation

The multi-walled carbon nanotubes (MWCNTs) were prepared using the chemical vapour deposition method (CVD), with acetylene as a carbon source and ferrocene as a source of iron, and were used as the catalytic material during the synthesis. The synthesis of the MWCNTs was performed at 850 °C. A scheme of the apparatus used during the CVD synthesis is presented in Figure 6. The obtained MWCNTs were then impregnated with an aqueous solution of palladium nitrate (V) and/or copper (II) nitrate trihydrate. Then, all catalysts were dried and calcined for four hours under static air at 350 °C. The metal loading was as follows: 20% wt. Cu, 1% wt. Pd, and 1% wt. Pd-20% wt. Cu.

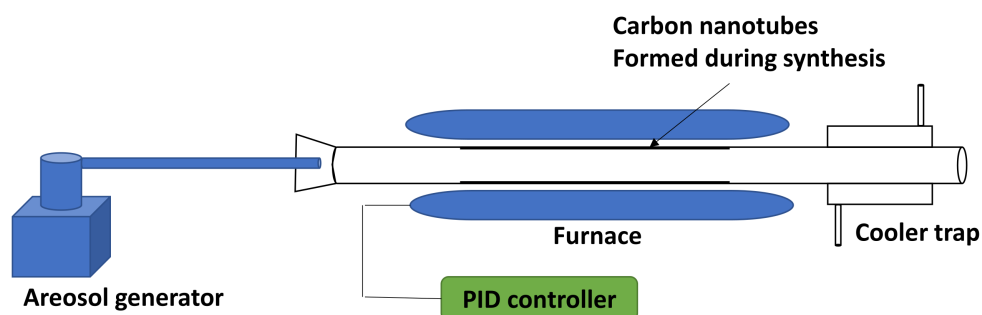


**Figure 6.** Scheme of the apparatus used during the CVD synthesis.

#### 3.2. Methods of Catalyst Characterization

The physicochemical properties of the synthesised catalysts were studied by using the TPR-H<sub>2</sub> and XRD methods (XRD, manufacturer, city, state abbrev if from USA, country), and the detailed description of these experiments had been presented in our previous work [40,57]. An FEI Quanta 450 FEG-ESEM equipped with an EDAX Apollo X energy-dispersive X-Ray (EDX, Hillsboro, OR, USA) was employed to investigate the morphology of the synthesised carbon nanotubes.

#### 3.3. Catalytic Activity Test

The catalytic activity during methanol steam reforming and methanol decomposition was measured using a quartz flow microreactor. About 0.1 g of the catalysts was loaded into the microreactor for the catalytic measurements. The reaction conditions of steam reforming of methanol were as follows: reaction temperature of 260–340 °C, a ratio of H<sub>2</sub>O:CH<sub>3</sub>OH = 1, a flow rate of 40 cm<sup>3</sup>/min, and atmospheric pressure. The methanol decomposition process was studied at two temperatures, 200 and 260 °C. The activity tests were performed for the catalysts calcined at 350 °C and for the catalytic systems that were calcined at 350 °C in the air for four hours and then reduced at 300 °C for 1 h in a mixture of 5% H<sub>2</sub>-95% Ar under atmospheric pressure. The results of the catalytic activity expressed as methanol conversion, selectivity to carbon monoxide and dioxide, and hydrogen yield in the studied processes were determined after the stabilisation of the catalytic system for 2 h at the tested temperature in a reaction mixture. The obtained results are the average of three analyses carried out for the organic and inorganic reaction products and reactants (methanol, methyl formate, dimethyl ether, formaldehyde, CO, CO<sub>2</sub>, and H<sub>2</sub>) using an on-line gas chromatography at each tested temperature. The precise description of the gas chromatography analysis had been presented in our earlier work [40].

### 4. Conclusions

Monometallic Cu, Pd, and bimetallic Pd-Cu catalysts were prepared on MWCNT support and tested during the steam reforming and decomposition of methanol. The 'spillover effect' between palladium and copper (II) oxide was confirmed during the reduction pro-

cess. The catalytic activity showed that multi-walled carbon nanotubes are a useful support material for metal catalysts in the studied reactions. The activity measurements showed that a 20 wt.% Cu catalyst promoted by palladium was the most active in the decomposition and steam reforming of methanol. At 300 °C, the order of the catalytic activity in the steam reforming and decomposition of methanol processes was as follows: Pd-Cu/MWCNT > Cu/MWCNT > Pd/MWCNT. Total conversion of methanol was achieved at 300 °C on the copper catalyst promoted by noble metal (Pd) during steam reforming of methanol and at 260 °C during decomposition of methanol. The highest activity observed for the Pd-Cu catalyst was due to the formation of a Pd-Cu alloy. These results show the potential of MWCNTs as a support material for various mono- and bimetallic catalysts.

**Author Contributions:** This work was designed and presented by P.M., A.M.-V., W.M., K.V. and M.S.-J. All authors have read and agreed to the published version of the manuscript.

**Funding:** This project was partially funded by the National Science Centre (Opus Programme—Grant No. 2018/29/B/ST8/01317) and (Sonata Programme—Grant No. DEC-2012/05/D/ST8/02856).

**Data Availability Statement:** All data supporting this study are available from authors upon request.

**Conflicts of Interest:** The authors declare no conflict of interest.

## References

1. Balat, M. Potential importance of hydrogen as a future solution to environmental and transportation problems. *Int. J. Hydrogen Energy* **2008**, *33*, 4013–4029. [\[CrossRef\]](#)
2. Viswanathan, B. Chapter 9—Hydrogen as an Energy Carrier. In *Energy Sources*; Elsevier: Amsterdam, The Netherlands, 2017; pp. 161–183.
3. Agrell, J.; Birgersson, H.; Boutonnet, M.; Melián-Cabrera, I.; Navarro, R.M.; Fierro, J.L.G. Production of hydrogen from methanol over Cu/ZnO catalysts promoted by ZrO<sub>2</sub> and Al<sub>2</sub>O<sub>3</sub>. *J. Catal.* **2003**, *219*, 389–403. [\[CrossRef\]](#)
4. Kayfeci, M.; Keçebaş, A.; Bayat, M. Chapter 3—Hydrogen production. In *Solar Hydrogen Production*; Calise, F., D’Accadia, M.D., Santarelli, M., Lanzini, A., Ferrero, D., Eds.; Academic Press: Cambridge, MA, USA, 2019; pp. 45–83.
5. Mierczynski, P. Comparative Studies of Bimetallic Ru–Cu, Rh–Cu, Ag–Cu, Ir–Cu Catalysts Supported on ZnO–Al<sub>2</sub>O<sub>3</sub>, ZrO<sub>2</sub>–Al<sub>2</sub>O<sub>3</sub> Systems. *Catal. Lett.* **2016**, *146*, 1825–1837. [\[CrossRef\]](#)
6. De Sá, M.H.; Pinto, A.M.F.R.; Oliveira, V.B. Passive Small Direct Alcohol Fuel Cells for Low-Power Portable Applications: Assessment Based on Innovative Increments since 2018. *Energies* **2022**, *15*, 3787. [\[CrossRef\]](#)
7. Mazloomi, K.; Gomes, C. Hydrogen as an energy carrier: Prospects and challenges. *Renew. Sustain. Energy Rev.* **2012**, *16*, 3024–3033. [\[CrossRef\]](#)
8. Cherry, R.S. A hydrogen utopia? *Int. J. Hydrogen Energy* **2004**, *29*, 125–129. [\[CrossRef\]](#)
9. Dash, S.K.; Chakraborty, S.; Roccotelli, M.; Sahu, U.K. Hydrogen Fuel for Future Mobility: Challenges and Future Aspects. *Sustainability* **2022**, *14*, 8285. [\[CrossRef\]](#)
10. Fan, L.; Tu, Z.; Chan, S.H. Recent development of hydrogen and fuel cell technologies: A review. *Energy Rep.* **2021**, *7*, 8421–8446. [\[CrossRef\]](#)
11. European Commission, K. *Hydrogen Energy and Fuel Cells a Vision of Our Future*; European Commission: Paris, France, 2003; p. 35.
12. Jeong, H.; Kim, K.I.; Kim, T.H.; Ko, C.H.; Park, H.C.; Song, I.K. Hydrogen production by steam reforming of methanol in a micro-channel reactor coated with Cu/ZnO/ZrO<sub>2</sub>/Al<sub>2</sub>O<sub>3</sub> catalyst. *J. Power Sources* **2006**, *159*, 1296–1299. [\[CrossRef\]](#)
13. Papavasiliou, J.; Avgouropoulos, G.; Ioannides, T. Combined steam reforming of methanol over Cu–Mn spinel oxide catalysts. *J. Catal.* **2007**, *251*, 7–20. [\[CrossRef\]](#)
14. Yong-Feng, L.; Xin-Fa, D.; Wei-Ming, L. Effects of ZrO<sub>2</sub>-promoter on catalytic performance of CuZnAlO catalysts for production of hydrogen by steam reforming of methanol. *Int. J. Hydrogen Energy* **2004**, *29*, 1617–1621. [\[CrossRef\]](#)
15. Ma, L.; Gong, B.; Tran, T.; Wainwright, M.S. Cr<sub>2</sub>O<sub>3</sub> promoted skeletal Cu catalysts for the reactions of methanol steam reforming and water gas shift. *Catal. Today* **2000**, *63*, 499–505. [\[CrossRef\]](#)
16. Clancy, P.; Breen, J.P.; Ross, J.R.H. The preparation and properties of coprecipitated Cu–Zr–Y and Cu–Zr–La catalysts used for the steam reforming of methanol. *Catal. Today* **2007**, *127*, 291–294. [\[CrossRef\]](#)
17. Yao, C.-Z.; Wang, L.-C.; Liu, Y.-M.; Wu, G.-S.; Cao, Y.; Dai, W.-L.; He, H.-Y.; Fan, K.-N. Effect of preparation method on the hydrogen production from methanol steam reforming over binary Cu/ZrO<sub>2</sub> catalysts. *Appl. Catal. A Gen.* **2006**, *297*, 151–158. [\[CrossRef\]](#)
18. Shen, J.-P.; Song, C. Influence of preparation method on performance of Cu/Zn-based catalysts for low-temperature steam reforming and oxidative steam reforming of methanol for H<sub>2</sub> production for fuel cells. *Catal. Today* **2002**, *77*, 89–98. [\[CrossRef\]](#)
19. Shishido, T.; Yamamoto, Y.; Morioka, H.; Takaki, K.; Takehira, K. Active Cu/ZnO and Cu/ZnO/Al<sub>2</sub>O<sub>3</sub> catalysts prepared by homogeneous precipitation method in steam reforming of methanol. *Appl. Catal. A Gen.* **2004**, *263*, 249–253. [\[CrossRef\]](#)

20. Jakdetchai, O.; Takayama, N.; Nakajima, T. Activity enhancement of CuZn-impregnated FSM-16 by modification with 1,3-butanediol for steam reforming of methanol. *Kinet. Catal.* **2005**, *46*, 56–64. [[CrossRef](#)]
21. Turco, M.; Bagnasco, G.; Cammarano, C.; Senese, P.; Costantino, U.; Sisani, M. Cu/ZnO/Al<sub>2</sub>O<sub>3</sub> catalysts for oxidative steam reforming of methanol: The role of Cu and the dispersing oxide matrix. *Appl. Catal. B Environ.* **2007**, *77*, 46–57. [[CrossRef](#)]
22. Kapoor, M.P.; Ichihashi, Y.; Kuraoka, K.; Shen, W.-J.; Matsumura, Y. Catalytic Methanol Decomposition Over Palladium Deposited on Mesoporous Cerium Oxide. *Catal. Lett.* **2003**, *88*, 83–87. [[CrossRef](#)]
23. Kapoor, M.P.; Ichihashi, Y.; Kuraoka, K.; Matsumura, Y. Catalytic methanol decomposition over palladium deposited on thermally stable mesoporous titanium oxide. *J. Mol. Catal. A Chem.* **2003**, *198*, 303–308. [[CrossRef](#)]
24. Velu, S.; Suzuki, K.; Okazaki, M.; Kapoor, M.P.; Osaki, T.; Ohashi, F. Oxidative Steam Reforming of Methanol over CuZnAl(Zr)-Oxide Catalysts for the Selective Production of Hydrogen for Fuel Cells: Catalyst Characterization and Performance Evaluation. *J. Catal.* **2000**, *194*, 373–384. [[CrossRef](#)]
25. Lenarda, M.; Moretti, E.; Storaro, L.; Patrono, P.; Pinzari, F.; Rodríguez-Castellón, E.; Jiménez-López, A.; Busca, G.; Finocchio, E.; Montanari, T.; et al. Finely dispersed Pd-Zn catalyst supported on an organized mesoporous alumina for hydrogen production by methanol steam reforming. *Appl. Catal. A Gen.* **2006**, *312*, 220–228. [[CrossRef](#)]
26. Usami, Y.; Kagawa, K.; Kawazoe, M.; Yasuyuki, M.; Sakurai, H.; Haruta, M. Catalytic methanol decomposition at low temperatures over palladium supported on metal oxides. *Appl. Catal. A Gen.* **1998**, *171*, 123–130. [[CrossRef](#)]
27. Mierczynski, P.; Mierczynska, A.; Ciesielski, R.; Mosinska, M.; Nowosielska, M.; Czyrkowska, A.; Maniukiewicz, W.; Szykowska, I.M.; Vasilev, K. High Active and Selective Ni/CeO<sub>2</sub>-Al<sub>2</sub>O<sub>3</sub> and Pd-Ni/CeO<sub>2</sub>-Al<sub>2</sub>O<sub>3</sub> Catalysts for Oxy-Steam Reforming of Methanol. *Catalysts* **2018**, *8*, 380. [[CrossRef](#)]
28. Chin, Y.-H.; Dagle, R.; Hu, J.; Dohnalkova, A.C.; Wang, Y. Steam reforming of methanol over highly active Pd/ZnO catalyst. *Catal. Today* **2002**, *77*, 79–88. [[CrossRef](#)]
29. Cubeiro, M.L.; Fierro, J.L.G. Selective Production of Hydrogen by Partial Oxidation of Methanol over ZnO-Supported Palladium Catalysts. *J. Catal.* **1998**, *179*, 150–162. [[CrossRef](#)]
30. Cubeiro, M.L.; Fierro, J.L.G. Partial oxidation of methanol over supported palladium catalysts. *Appl. Catal. A Gen.* **1998**, *168*, 307–322. [[CrossRef](#)]
31. Liao, P.-H.; Yang, H.-M. Preparation of Catalyst Ni-Cu/CNTs by Chemical Reduction with Formaldehyde for Steam Reforming of Methanol. *Catal. Lett.* **2008**, *121*, 274–282. [[CrossRef](#)]
32. Serp, P.; Corrias, M.; Kalck, P. Carbon nanotubes and nanofibers in catalysis. *Appl. Catal. A Gen.* **2003**, *253*, 337–358. [[CrossRef](#)]
33. Seelam, P.K.; Huuhtanen, M.; Sápi, A.; Szabó, M.; Kordás, K.; Turpeinen, E.; Tóth, G.; Keiski, R.L. CNT-based catalysts for H<sub>2</sub> production by ethanol reforming. *Int. J. Hydrogen Energy* **2010**, *35*, 12588–12595. [[CrossRef](#)]
34. Pham-Huu, C.; Keller, N.; Ehret, G.; Charbonniere, L.C.J.; Ziessel, R.; Ledoux, M.J. Carbon nanofiber supported palladium catalyst for liquid-phase reactions: An active and selective catalyst for hydrogenation of cinnamaldehyde into hydrocinnamaldehyde. *J. Mol. Catal. A Chem.* **2001**, *170*, 155–163. [[CrossRef](#)]
35. Hou, T.; Yuan, L.; Ye, T.; Gong, L.; Tu, J.; Yamamoto, M.; Torimoto, Y.; Li, Q. Hydrogen production by low-temperature reforming of organic compounds in bio-oil over a CNT-promoting Ni catalyst. *Int. J. Hydrogen Energy* **2009**, *34*, 9095–9107. [[CrossRef](#)]
36. Solhy, A.; Machado, B.F.; Beausoleil, J.; Kihn, Y.; Gonçalves, F.; Pereira, M.F.R.; Órfão, J.J.M.; Figueiredo, J.L.; Faria, J.L.; Serp, P. MWCNT activation and its influence on the catalytic performance of Pt/MWCNT catalysts for selective hydrogenation. *Carbon* **2008**, *46*, 1194–1207. [[CrossRef](#)]
37. Tessonnier, J.-P.; Pesant, L.; Ehret, G.; Ledoux, M.J.; Pham-Huu, C. Pd nanoparticles introduced inside multi-walled carbon nanotubes for selective hydrogenation of cinnamaldehyde into hydrocinnamaldehyde. *Appl. Catal. A Gen.* **2005**, *288*, 203–210. [[CrossRef](#)]
38. Tang, J.M.; Jensen, K.; Waje, M.; Li, W.; Larsen, P.; Pauley, K.; Chen, Z.; Ramesh, P.; Itkis, M.E.; Yan, Y.; et al. High Performance Hydrogen Fuel Cells with Ultralow Pt Loading Carbon Nanotube Thin Film Catalysts. *J. Phys. Chem. C* **2007**, *111*, 17901–17904. [[CrossRef](#)]
39. Liu, Z.-T.; Wang, C.-X.; Liu, Z.-W.; Lu, J. Selective hydrogenation of cinnamaldehyde over Pt-supported multi-walled carbon nanotubes: Insights into the tube-size effects. *Appl. Catal. A Gen.* **2008**, *344*, 114–123. [[CrossRef](#)]
40. Mierczynski, P.; Mierczynska, A.; Maniukiewicz, W.; Maniecki, T.P.; Vasilev, K. MWCNTs as a catalyst in oxy-steam reforming of methanol. *RSC Adv.* **2016**, *6*, 81408–81413. [[CrossRef](#)]
41. Moen, A.; Nicholson, D.G.; Rønning, M.; Emerich, H. In situ X-ray absorption spectroscopic studies at the cobalt K-edge on an Al<sub>2</sub>O<sub>3</sub>-supported rhenium-promoted cobalt Fischer-Tropsch catalyst. Comparing reductions in high and low concentration hydrogen. *J. Mater. Chem.* **1998**, *8*, 2533–2539. [[CrossRef](#)]
42. Neyertz, C.; Marchesini, F.A.; Boix, A.; Miró, E.; Querini, C.A. Catalytic reduction of nitrate in water: Promoted palladium catalysts supported in resin. *Appl. Catal. A Gen.* **2010**, *372*, 40–47. [[CrossRef](#)]
43. Mierczynski, P.; Vasilev, K.; Mierczynska, A.; Maniukiewicz, W.; Maniecki, T.P. Highly selective Pd-Cu/ZnAl<sub>2</sub>O<sub>4</sub> catalyst for hydrogen production. *Appl. Catal. A Gen.* **2014**, *479*, 26–34. [[CrossRef](#)]
44. Xiong, H.; Motchelaho, M.A.M.; Moyo, M.; Jewell, L.L.; Coville, N.J. Correlating the preparation and performance of cobalt catalysts supported on carbon nanotubes and carbon spheres in the Fischer-Tropsch synthesis. *J. Catal.* **2011**, *278*, 26–40. [[CrossRef](#)]

45. Lambert, S.; Heinrichs, B.T.; Brasseur, A.; Rulmont, A.; Pirard, J.-P. Determination of surface composition of alloy nanoparticles and relationships with catalytic activity in Pd–Cu/SiO<sub>2</sub> cogelled xerogel catalysts. *Appl. Catal. A Gen.* **2004**, *270*, 201–208. [[CrossRef](#)]
46. Trawczyński, J.; Gheek, P.; Okal, J.; Zawadzki, M.; Gomez, M.J.I. Reduction of nitrate on active carbon supported Pd–Cu catalysts. *Appl. Catal. A Gen.* **2011**, *409–410*, 39–47. [[CrossRef](#)]
47. Sun, K.; Liu, J.; Nag, N.K.; Browning, N.D. Atomic Scale Characterization of Supported Pd–Cu/ $\gamma$ -Al<sub>2</sub>O<sub>3</sub> Bimetallic Catalysts. *J. Phys. Chem. B* **2002**, *106*, 12239–12246. [[CrossRef](#)]
48. Shen, H.; Li, H.; Yang, Z.; Li, C. Magic of hydrogen spillover: Understanding and application. *Green Energy Environ.* **2022**, *7*, 1161–1198. [[CrossRef](#)]
49. Günter, M.M.; Ressler, T.; Jentoft, R.E.; Bems, B. Redox Behavior of Copper Oxide/Zinc Oxide Catalysts in the Steam Reforming of Methanol Studied by in Situ X-Ray Diffraction and Absorption Spectroscopy. *J. Catal.* **2001**, *203*, 133–149. [[CrossRef](#)]
50. Jones, S.D.; Hagelin-Weaver, H.E. Steam reforming of methanol over CeO<sub>2</sub>- and ZrO<sub>2</sub>-promoted Cu–ZnO catalysts supported on nanoparticle Al<sub>2</sub>O<sub>3</sub>. *Appl. Catal. B Environ.* **2009**, *90*, 195–204. [[CrossRef](#)]
51. Song, S.; Jiang, S. Selective catalytic oxidation of ammonia to nitrogen over CuO/CNTs: The promoting effect of the defects of CNTs on the catalytic activity and selectivity. *Appl. Catal. B Environ.* **2012**, *117–118*, 346–350. [[CrossRef](#)]
52. Chen, W.; Fan, Z.; Pan, X.; Bao, X. Effect of Confinement in Carbon Nanotubes on the Activity of Fischer–Tropsch Iron Catalyst. *J. Am. Chem. Soc.* **2008**, *130*, 9414–9419. [[CrossRef](#)]
53. Mierczynski, P.; Vasilev, K.; Mierczynska, A.; Maniukiewicz, W.; Szyrkowska, M.I.; Maniecki, T.P. Bimetallic Au–Cu, Au–Ni catalysts supported on MWCNTs for oxy-steam reforming of methanol. *Appl. Catal. B Environ.* **2016**, *185*, 281–294. [[CrossRef](#)]
54. Mierczynski, P.; Vasilev, K.; Mierczynska, A.; Maniukiewicz, W.; Ciesielski, R.; Rogowski, J.; Szyrkowska, I.M.; Trifonov, A.Y.; Dubkov, S.V.; Gromov, D.G.; et al. The effect of gold on modern bimetallic Au–Cu/MWCNT catalysts for the oxy-steam reforming of methanol. *Catal. Sci. Technol.* **2016**, *6*, 4168–4183. [[CrossRef](#)]
55. Schuyten, S.; Guerrero, S.; Miller, J.T.; Shibata, T.; Wolf, E.E. Characterization and oxidation states of Cu and Pd in Pd–CuO/ZnO/ZrO<sub>2</sub> catalysts for hydrogen production by methanol partial oxidation. *Appl. Catal. A Gen.* **2009**, *352*, 133–144. [[CrossRef](#)]
56. Nomoto, K.; Kubo, Y.; Miura, H.; Shishido, T. Production of Hydrogen by the Autothermal Reforming of Methanol over Cu/ZnO/Al<sub>2</sub>O<sub>3</sub>-based Catalysts: Improved Durability and Self-activation Ability upon Pd-doping. *J. Jpn. Pet. Inst.* **2022**, *65*, 161–170. [[CrossRef](#)]
57. Mierczynski, P.; Ciesielski, R.; Kedziora, A.; Nowosielska, M.; Kubicki, J.; Maniukiewicz, W.; Czyrkowska, A.; Maniecki, T.P. Monometallic copper catalysts supported on multi-walled carbon nanotubes for the oxy-steam reforming of methanol. *React. Kinet. Mech. Catal.* **2016**, *117*, 675–691. [[CrossRef](#)]

**Disclaimer/Publisher’s Note:** The statements, opinions and data contained in all publications are solely those of the individual author(s) and contributor(s) and not of MDPI and/or the editor(s). MDPI and/or the editor(s) disclaim responsibility for any injury to people or property resulting from any ideas, methods, instructions or products referred to in the content.